

Photonic band gap enhancement in frequency-dependent dielectrics

Ovidiu Toader and Sajeev John

Department of Physics, University of Toronto, 60 St. George Street, Toronto, Ontario, Canada M5S 1A7

(Received 9 October 2003; revised manuscript received 21 May 2004; published 11 October 2004)

We illustrate a general technique for evaluating photonic band structures in periodic d -dimensional microstructures in which the dielectric constant $\epsilon(\omega)$ exhibits rapid variations with frequency ω . This technique involves the evaluation of generalized electromagnetic dispersion surfaces $\omega(\vec{k}, \epsilon)$ in a $(d+1)$ -dimensional space consisting of the physical d -dimensional space of wave vectors \vec{k} and an additional dimension defined by the continuous, independent, variable ϵ . The physical band structure for the photonic crystal is obtained by evaluating the intersection of the generalized dispersion surfaces with the “cutting surface” defined by the function $\epsilon(\omega)$. We apply this method to evaluate the band structure of both two- and three-dimensional (3D) periodic microstructures. We consider metallic photonic crystals with free carriers described by a simple Drude conductivity and verify the occurrence of electromagnetic pass bands below the plasma frequency of the bulk metal. We also evaluate the shift of the photonic band structure caused by free carrier injection into semiconductor-based photonic crystals. We apply our method to two models in which $\epsilon(\omega)$ describes a resonant radiation-matter interaction. In the first model, we consider the addition of independent, resonant oscillators to a photonic crystal with an otherwise frequency-independent dielectric constant. We demonstrate that for an inhomogeneously broadened distribution of resonators impregnated within an inverse opal structure, the full 3D photonic band gap (PBG) can be considerably enhanced. In the second model, we consider a coupled resonant oscillator mode in a photonic crystal. When this mode is an optical phonon, there can be a synergetic interplay between the polaritonic resonance and the geometrical scattering resonances of the structured dielectric, leading to PBG enhancement. A similar effect may arise when resonant atoms that are coupled radiatively through resonance dipole-dipole interaction are placed in a photonic crystal.

DOI: 10.1103/PhysRevE.70.046605

PACS number(s): 42.70.Qs

I. INTRODUCTION

Photonic band gap (PBG) materials [1,2] are engineered periodic structures which facilitate the localization of light [3]. The study of PBG's in three-dimensional (3D) periodic materials has focused primarily on materials for which the dielectric constant is independent of frequency. In this case, a PBG arises from the interplay of two geometrical effects. The first is a macroscopic (Bragg) scattering resonance associated with periodicity of the dielectric microstructure. The second is the microscopic scattering resonance of the dielectric structure in a single unit cell of the periodic system. If the refractive index contrast across the dielectric interfaces is sufficiently large and the scattering geometry is carefully chosen (so that both resonances occur at a common frequency), a complete absence of electromagnetic wave propagation in any direction over a finite frequency interval may occur. The mathematical problem of band gap formation can be solved as a linear eigenvalue problem obtained from Maxwell's equations [4]. A minimum refractive index ratio of about 2.0 [4] is required for PBG formation in even the most ideal geometries such as the diamond lattice. In less ideal structures, the minimum index ratio may be closer to 3.0. This places severe constraints on the types of materials and geometries that are amenable to PBG formation. We demonstrate, in this paper, that the photonic band gap of 3D PBG materials can be enhanced when the underlying dielectric constant is allowed to vary appropriately with frequency.

Electronic and vibrational excitations in a material may interact resonantly with an electromagnetic wave and dra-

matically alter its propagation through the medium. A simple example is that of electronic free carriers in a metal with a bulk plasma frequency below which electromagnetic waves are screened and cannot propagate. This can be described using a frequency-dependent Drude dielectric function [5]. In a metallic photonic crystal with a connected air component, it is possible for photons of certain narrow frequency ranges below the plasma frequency to be guided through air, resulting in pass bands. These effects have been studied in 2D photonic crystals by Maradudin and co-workers [6–9] and Sakoda and co-workers [10–12]. Band structure results for realistic 3D metallic photonic crystals are much less developed [13–15]. Recent experiments on a 3D tungsten-based photonic crystal have suggested that the occurrence of band gaps and pass bands may modify the blackbody radiation emitted by the crystal when it is heated by passage of an electrical current [16]. The observed redistribution of heat into higher-frequency light may be very important for efficient lighting technologies.

Another realization of free carriers in a semiconductor-based photonic crystal occurs in photoelectrochemically etched macroporous silicon [17–19]. Here, the fabrication procedure itself leads to the presence of residual free carriers whose concentration varies with the porosity (air to silicon volume fraction ratio). Recently, ultrafast tuning of band structure has been demonstrated in such photonic crystals performed by optical injection of electron-hole pairs [20]. Band structure calculations in 2D [21,22] have likewise predicted the shift of certain electromagnetic dispersion curves with free carrier concentration. In all these cases, the under-

lying dielectric constant acquires a Drude-like frequency dependence.

If certain electronic degrees of freedom in the photonic crystal are confined rather than free, a different type of frequency dependence to the dielectric constant can be obtained. For example, a quantum dot can exhibit a ground to electronic excited state transition in resonance with an electromagnetic wave in the photonic crystal. If the crystal is impregnated with a high concentration of such resonators, then the dielectric constant will exhibit rapid variations with frequency in the vicinity of the resonance leading to dramatic changes in the electromagnetic wave characteristics. For frequencies slightly below the resonance, the real part of the dielectric constant is enhanced whereas slightly above the resonance the real part is suppressed. This effect is particularly important when the resonance frequency is placed inside a stop gap of the photonic crystal. The higher dielectric constant near the lower edge of the stop gap will tend to move the band edge to lower frequency, whereas the lower dielectric constant near the upper edge of the stop gap will tend to move this band edge to higher frequency. The net result is that the overall stop gap is enhanced. A similar effect occurs in a material with an incipient photonic band gap. By placing a carefully chosen concentration of resonators in precise locations, it is possible to open a complete PBG where one would not appear otherwise. Alternatively, by adding resonators in a prescribed manner to a material with a relatively small PBG, it is possible to increase the size of the overall 3D PBG considerably. This is illustrated through a model in which colloidal quantum dots are coated on the inner surfaces of a silicon-based inverse opal structure [23]. Similar effects may occur with the infiltration of dye molecules into photonic crystals [24,25]. Since the highly dispersive real part of the dielectric constant is accompanied by a resonance peak in the imaginary part, it is important to carefully consider damping and absorption effects associated with this mechanism for PBG enhancement. We suggest that, if the absorption frequency of an isolated resonator falls within the PBG, it leads to localized states of light within the PBG [26]. If the resonators are sufficiently strongly coupled to one another, energy transfer can take place within the PBG through the ‘‘impurity band’’ created by the resonators. In our computational approach based on a ‘‘cutting surface method’’ (CSM), we neglect the imaginary part of the dielectric constant. In the region of anomalous dispersion, $d\text{Re}[\varepsilon(\omega)]/d\omega < 0$, this may lead to the phenomenon of ‘‘wave vector gaps’’ (WVG’s) accompanied by dispersion bubbles (closed curves in the band structure diagram) where $d\omega/dk$ appears unbounded at certain points. Causality, however, may be recaptured through an appropriate analysis of the role of the imaginary part of the dielectric constant.

In Sec. II we define the problem of calculating the photonic band structure in the presence of a frequency-dependent dielectric and introduce the most frequently used models of dielectric constants. This is followed in Sec. III by a detailed description of our method for evaluating the corresponding photonic band structure. We present results for various two-dimensional photonic crystals in Sec. IV. This is followed by results for three-dimensional photonic crystals in Sec. V. A discussion and interpretation of wave vector gaps is given in Sec. VI, followed by concluding remarks in Sec. VII.

II. PHOTONIC BAND STRUCTURE IN THE PRESENCE OF FREQUENCY-DEPENDENT DIELECTRICS

The photonic band structure of a perfect photonic crystal is determined by the eigenvalues of the following familiar equation [27]:

$$\vec{\nabla} \times [\varepsilon^{-1}(\vec{r}, \omega) \vec{\nabla} \times \vec{H}_\omega(\vec{r})] = \left(\frac{\omega}{c}\right)^2 \vec{H}_\omega(\vec{r}) \quad (1)$$

where $\varepsilon(\vec{r}, \omega)$ is the dielectric constant of the crystal and $\vec{H}_\omega(\vec{r})$ is the monochromatic component (of frequency ω) of the magnetic field, which satisfies the Bloch condition [27]

$$\vec{H}_\omega(\vec{r}) = e^{i\vec{k}_b \cdot \vec{r}} \vec{H}_{\vec{k}_b, \omega}(\vec{r}). \quad (2)$$

\vec{k}_b is the Bloch vector lying in the first Brillouin zone of the crystal’s reciprocal space and $\vec{H}_{\vec{k}_b, \omega}(\vec{r})$ has the same periodicity as the underlying Bravais lattice. When regarded as an eigenvalue problem for the frequency ω , Eq. (1) has a nonlinear character because the dielectric constant $\varepsilon(\vec{r}, \omega)$, which acts as a scattering potential, itself depends on the eigenvalue ω . We refer to this as a nonlinear eigenvalue problem. An analytic solution of Eq. (1) for an arbitrary $\varepsilon(\vec{r}, \omega)$ is possible in the case of a one-dimensional periodic grating (see the Appendix for details). In two and three dimensions there has been no general prescription up to now (nor a reliable numerical method) for determining the solution of Eq. (1) for an arbitrary $\varepsilon(\vec{r}, \omega)$.¹

A few commonly used dielectric functions are listed below.

(1) The dielectric constant of a conducting solid can be approximated very well [28] by the Drude formula

$$\varepsilon(\omega) = \varepsilon_0 \left(1 - \frac{\omega_p^2}{\omega(\omega + i\tau^{-1})} \right) \quad (3)$$

where ω_p and τ are the plasma frequency and relaxation time of the conducting electrons, respectively. ε_0 is 1 for a pure metal but can be different from 1 for a semiconductor.

(2) The dielectric constant of a dilute collection of resonant absorbers (molecules, quantum dots, or other impurities) is given by

$$\varepsilon(\omega) = 1 + \frac{4\pi N e^2}{m} \sum_j \frac{f_j}{\omega_j^2 - \omega^2 - i\omega\gamma_j} \quad (4)$$

where N is the number of molecules per unit volume, Z is the number of electrons per molecule, and f_j is the number of electrons per molecule which have the resonant frequency and damping coefficient ω_j and γ_j , respectively. f_j , the oscillator strengths, satisfy $\sum_j f_j = Z$. Here it is assumed that the damping rates γ_j are larger than the rate of direct energy

¹The determinantal approach described later can be used to solve the general Eq. (1) but it requires a very large amount of computations. The transfer matrix method described in [13] can in principle be used to calculate the photonic band structure for an arbitrary $\varepsilon(\vec{r}, \omega)$. However, the computational algorithm in this case is not stable numerically.

transfer between oscillators, so that each oscillator can be considered independent.

(3) Insulating solids, without extrinsic impurities, can also exhibit highly dispersive properties in the frequency range of an intrinsic, elementary excitation which interacts strongly with light. The elementary excitation is a specific case of strongly coupled resonators which can exchange energy among themselves within the solid. For instance, in polar crystals the dielectric constant is given by [29]

$$\varepsilon(\omega) = \varepsilon_\infty + (\varepsilon_0 - \varepsilon_\infty) \frac{\omega_T^2}{\omega_T^2 - \omega^2 - i\gamma\omega} \quad (5)$$

where ω_T is the transverse optical phonon frequency, γ is the absorption coefficient, and $\varepsilon_0, \varepsilon_\infty$ are the dielectric constants at low and high frequencies, respectively. If one neglects the absorption ($\gamma=0$) Eq. (5) can be rewritten in the more familiar form

$$\varepsilon(\omega) = \varepsilon_\infty \frac{\omega_L^2 - \omega^2}{\omega_T^2 - \omega^2} \quad (6)$$

where $\omega_L^2 = \omega_T^2 \varepsilon_0 / \varepsilon_\infty$ (Lyddane-Sachs-Teller relation). This strong resonance at the optical phonon frequency is associated with the formation of a polariton, a hybrid excitation involving both the electromagnetic and vibrational modes of the solid. Solids exhibiting this type of dielectric constant include GaAs, InP, NaCl, and KCl.

In view of the variety of different frequency-dependent dielectric functions, it is useful to develop a general method to solve Eq. (1) for an arbitrary $\varepsilon(\vec{r}, \omega)$. In the next section we introduce such a method.

For a frequency independent dielectric (FID) constant Eq. (1) can be mapped [4,30] directly into an ordinary eigenvalue equation for an infinite Hermitian (or symmetric) matrix $\hat{M}\vec{h} = (\omega/c)^2 \vec{h}$ where \hat{M} (independent of ω) is the matrix representation of the left hand side of Eq. (1) in a plane wave basis and \vec{h} is the eigenvector whose elements are the expansion coefficients in this basis. This eigensystem (after truncation to a finite size) can be calculated using well established numerical algorithms. We call the band structure obtained in this case an *ordinary* photonic band structure.

If one is interested only in the eigenfrequencies of Eq. (1) then a determinantal approach to calculating the photonic band structure can be used [6]. The eigenfrequencies in this case are obtained as the frequencies at which the determinant of $\hat{M}(\omega) - (\omega/c)^2 \hat{1}$ is zero. The dependence of \hat{M} on ω comes entirely from the dielectric constant. This approach to solving the eigenfrequencies of Eq. (1) is seldom used in practice due to the large number of floating point operations required.

There are a few specific cases where specialized techniques have been employed to evaluate the photonic band structure of frequency-dependent dielectrics. For a 2D photonic crystal, in the absence of dissipation ($\tau = \infty$), the frequency dependence given by Eq. (3) enables a mapping of Eq. (1) to an ordinary eigenvalue problem [6,7], which can be solved using the plane wave method. An extension to the case of finite τ is presented in Ref. [8]. The photonic band structure of a fcc crystal made from spheres whose dielectric

constant is given by Eq. (3) was calculated in Ref. [6] using a root finding technique and in Ref. [31] using a photonic analog of the Korringa-Kohn-Rostoker method [32]. The photonic band structure for 2D photonic crystals described by the Drude model, Eq. (3), has been calculated in Refs. [22,33,34]. Finally, the polaritonic frequency dependence given by Eq. (6) also allows a special treatment in the 2D case, leading to a generalized eigenvalue problem [35]. In Ref. [36] the corresponding 2D band structure has been obtained using a determinantal approach.

III. "CUTTING SURFACE" METHOD OF BAND STRUCTURE CALCULATION

In this section we introduce a fundamental and general method of calculating band structures of photonic crystals of arbitrary structure, dimensionality, and frequency-dependent functions $\varepsilon(\omega)$. We first illustrate our method using a one-dimensional model and compare the results to a semianalytical solution. As we demonstrate below, our "cutting surface" method extends straightforwardly to two- and three-dimensional photonic crystals. In order to make the generality of the method more apparent, we choose to display the one-dimensional Bloch vector in bold face (\mathbf{k}_b).

Consider a one-dimensional photonic crystal whose unit cell consists of two layers characterized by [dielectric, thickness] of $[\varepsilon_1, d_1]$ and $[\varepsilon_2, d_2]$, respectively (see Fig. 26 in the Appendix). The calculation of the photonic band structure in this case is described in detail in the Appendix. For a given Bloch vector \mathbf{k}_b , the frequencies of all the modes are determined by the solution of Eq. (A5); this can be solved even when the dielectric constant has an explicit frequency dependence. For concreteness we assume $d_1/|a|=0.2$, $\varepsilon_2=1$, and $\varepsilon_1(\omega_s)=10 \sin(4\omega_s)$ where ω_s denotes the scaled frequency introduced by Eq. (A6). The "unphysical" and extreme expression for $\varepsilon_1(\omega)$ is chosen to illustrate the mathematical correctness of the method. Once this one-dimensional, mathematical, test case is explored in detail, the broad applicability of the method to "physical" systems will become apparent.

Figure 27 in the Appendix shows the photonic band structure of the one-dimensional photonic crystal described above. The frequencies of the bands are the solutions of Eq. (1) and Eq. (2) in the 1D case and have been determined by the solutions of the transcendental Eq. (A5) with the proper parameters in place. This is a practically exact photonic band structure.

To illustrate our method, we consider a set of photonic band structures for this 1D crystal in which the solid component is replaced by a frequency-independent dielectric. Each photonic band structure corresponds to the following parameters: $|d_1/|a|=0.2$, $\varepsilon_2=1$, and $\varepsilon_1=\varepsilon$ where ε runs in a finite range $[\varepsilon_{\min}, \varepsilon_{\max}]$. The only parameter that changes from band structure to band structure is ε , the dielectric constant of the solid component. The geometry of the photonic crystal is identical to the one used in the Appendix. Figure 1 displays the first band of this photonic crystal calculated for a discrete set of ε values, running from -11 to $+11$ in steps of 1, with the exception of the interval $[-6, -3]$ where the

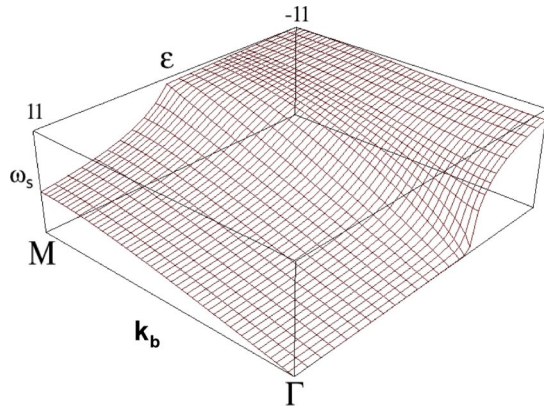


FIG. 1. 1D bands for a series of FID's. The photonic crystal is characterized by $\varepsilon_1=\varepsilon$, $\varepsilon_2=1$, and $|d|_1/|a|=0.2$. The value of the dielectric constant of the first layer varies from -11 to $+11$ in steps of 1 with the exception of the interval $[-6, -3]$ where a step of 0.5 was chosen. In each case the lowest band of the 1D photonic band structure was calculated (i.e., $\omega_s^{(1)}$ versus \mathbf{k}_b). The $\mathbf{k}_b=\text{const}$ lines are displayed as a visual guide for the reader.

step is 0.5. The functional form of the first band of the photonic band structure is denoted by $\omega_s^{(1)}(\mathbf{k}_b; \varepsilon)$ which indicates that $\omega_s^{(1)}$ is a continuous function of \mathbf{k}_b and depends parametrically on ε . Γ and M correspond to $\mathbf{k}_b=0$ and $\mathbf{k}_b=\pi/|a|$, respectively. The cutoff frequency at the Γ point that is visible in Fig. 1 appears when $\varepsilon < -4$ [see Eq. (A10)].

As seen in Fig. 1 the dependence of $\omega_s^{(1)}$ on ε for a given \mathbf{k}_b is relatively smooth. The only area in the $(\mathbf{k}_b, \varepsilon)$ space where this dependence is not as smooth is for the first band around Γ and ε where the cutoff sets in. For the higher bands or the rest of the $(\mathbf{k}_b, \varepsilon)$ space the frequency of the band is a slowly varying monotonically decreasing function of ε . Based on this observation, we can now extend by interpolation the one-dimensional, parametric function $\omega_s^{(1)}(\mathbf{k}_b; \varepsilon)$ to a two-dimensional function $\omega_s^{(1)}(\mathbf{k}_b, \varepsilon)$ which now depends continuously on both \mathbf{k}_b and ε . We call this function the first band surface.

In order to find the frequencies of the first band for, say, $\varepsilon=7.25$, we interpolate between the frequencies calculated for $\varepsilon=7$, $\omega_s^{(1)}(\mathbf{k}_b, 7)$, and $\varepsilon=8$, $\omega_s^{(1)}(\mathbf{k}_b, 8)$. This procedure is equivalent to calculating the intersection between the band surface $\omega_s^{(1)}(\mathbf{k}_b, \varepsilon)$ and the plane defined by $\varepsilon=7.25$ in the $(\mathbf{k}_b, \varepsilon, \omega_s)$ space. Figure 2 shows the first four band surfaces and their intersection with the plane $\varepsilon=7.25$. The surfaces are slightly transparent and have different colors. By sweeping the “cutting” plane along the ε axis in Fig. 2 we obtain (with very good accuracy) the photonic band structures of the family of FID's for all the values of ε in the range of available data (which in this case is $-11 \leq \varepsilon \leq 11$).

In order to treat a frequency-dependent dielectric (FDD) we use a different surface to “cut” through the band surfaces. The new “cutting” surface is defined implicitly by the function $\varepsilon(\omega_s, \mathbf{k}_b)=10 \sin(4\omega_s)$. The dependence of this implicit function on \mathbf{k}_b is trivial but it illustrates that we are dealing with a surface in a 3D space [the space defined by the parameters $(\mathbf{k}_b, \varepsilon, \omega_s)$]. Figure 3 displays this “cutting” surface together with the first two band surfaces of our model pho-

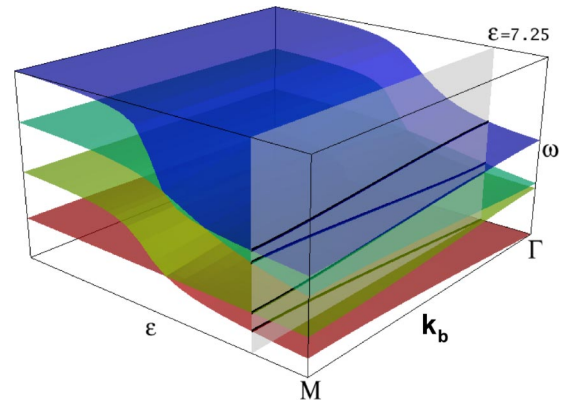


FIG. 2. (Color online) The frequency of the lowest four bands for $\varepsilon=7.25$ can be determined by the intersection of the $\varepsilon=7.25$ plane in the $(\mathbf{k}_b, \varepsilon, \omega_s)$ space with the four lowest band surfaces obtained by interpolating between the $\varepsilon=\text{const}$ bands previously calculated. For a description of the axes see the caption of Fig. 1.

tonic crystal. The intersections between the “cutting” surface and the bands are also highlighted. The essence of our method of calculating photonic band structures of frequency-dependent dielectrics is the following: the projection on the (\mathbf{k}_b, ω_s) plane of the intersections between the “cutting” surface and the band surfaces consists of points (\mathbf{k}_b, ω) which satisfy Eqs. (1) and (2) when the dielectric constant has the corresponding frequency dependence. In this particular case the (\mathbf{k}_b, ω) pairs satisfy Eq. (1) when $\varepsilon_1(\omega_s, \mathbf{k}_b)=10 \sin(4\omega_s)$, $\varepsilon_2=1$, and $|d|_1/|a|=0.2$.

Calculating the photonic band structure for a different dielectric function requires only the replacement of the “cutting” surface defined by $\varepsilon(\omega_s, \mathbf{k}_b)=10 \sin(4\omega_s)$ with $\varepsilon(\omega_s, \mathbf{k}_b)=\varepsilon(\omega_s)$, where $\varepsilon(\omega_s)$ is an arbitrary real function. This function need not have a simple analytic form but could be taken from an experimental data set. The amount of computation required to calculate these intersections is negligible, and therefore studying the change of the photonic band structure caused by a change in $\varepsilon(\omega)$ becomes an almost real-time process. In the case of a 1D photonic crystal, the cutting surface method produces a band structure projected on the (\mathbf{k}_b, ω_s) plane that is practically indistinguishable from the exact analytical calculation, Fig. 27 below.

We mention briefly the factors that affect the overall accuracy of the calculations involved in the procedure described above. There are two sources of potential numerical errors. First is the interpolation error used to generate the band surface from the separate bands (see Fig. 1). This error can be controlled easily by calculating the FID bands for more ε values in regions where $\omega_s^{(n)}(\mathbf{k}_b, \varepsilon)$ displays a strong variation with ε . The second source of error comes from the calculation of the intersection between the “cutting” surface and the band surface. As long as the functional form of the frequency dependence of the dielectric constant is known accurately, this type of error can easily be reduced to an order of magnitude lower than the other errors.

The extension of the CSM to the case of 2D and 3D photonic crystals is straightforward. Consider a two-component photonic crystal characterized by dielectric con-

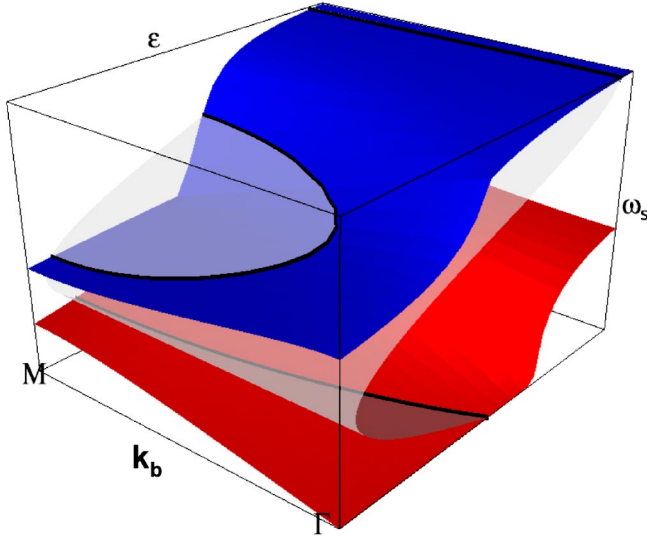


FIG. 3. (Color online) The solution of the band structure calculation for a FDD. Here we use the “cutting” surface defined implicitly by $\varepsilon(\omega_s, \mathbf{k}_b) = 10 \sin(4\omega_s)$ whose intersections with the lowest two band surfaces are calculated. The projection of these intersections on the (\mathbf{k}_b, ω_s) plane is identical with the lowest three bands displayed in Fig. 27 below. For a description of the axes see the caption of Fig. 1.

stant $\varepsilon_1(\omega) = 1$ in the first component and $\varepsilon_2(\omega) = \varepsilon(\omega)$ in the second. By using Eq. (2) in Eq. (1) we obtain the following eigenvalue problem for the H field:

$$(i\vec{k}_b + \vec{\nabla}) \times [\varepsilon^{-1}(\vec{r}, \omega)(i\vec{k}_b + \vec{\nabla}) \times \vec{H}_{\vec{k}_b, \omega}(\vec{r})] = \left(\frac{\omega}{c}\right)^2 \vec{H}_{\vec{k}_b, \omega}(\vec{r}). \quad (7)$$

We define $\omega_s^{(n)}(\vec{k}_b; \varepsilon)$ as the n th eigenfrequency of Eq. (7) corresponding to Bloch vector \vec{k}_b when $\varepsilon(\vec{r}, \omega) = 1$ in the first component and $\varepsilon_2(\vec{r}, \omega) = \varepsilon$, a constant independent of ω , in the second component. $\omega_s^{(n)}(\vec{k}_b; \varepsilon)$ can be calculated using standard photonic band structure methods since we have temporarily replaced $\varepsilon(\vec{r}, \omega)$ with a FID. The dashed line in Fig. 4 shows the frequency of this particular band, $\omega_s^{(n)}(\vec{k}_b; \varepsilon)$, as a function of ε when both n and \vec{k}_b are fixed. The continuous curve represents the value of the dielectric of the

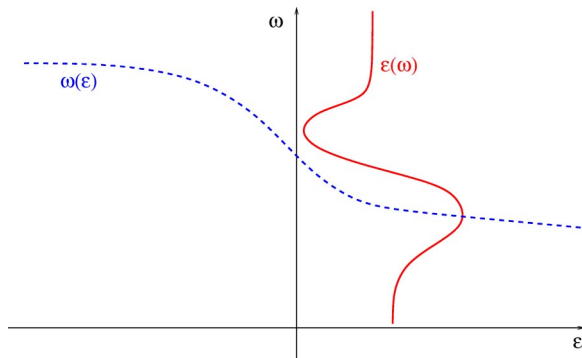


FIG. 4. (Color online) Graphical solution of Eq. (7). The dashed curve represents the frequency of a certain band \mathbf{n}_b for a fixed Bloch vector \vec{k}_b as a function of the dielectric constant of the second component. The continuous curve represents the dielectric constant of the second component as a function of frequency. The intersections between the two curves are the frequencies of allowed modes of Bloch vector \vec{k}_b which all satisfy Eq. (7) when $\varepsilon_2(\omega) = \varepsilon(\omega)$.

second component ε_2 as a function of ω . The intersections between the two curves provide a set of frequencies that satisfy Eq. (7) when the dielectric constant of the second component has an explicit frequency dependence given by $\varepsilon_2(\omega)$. We note that, in general, more than one intersection between the band surface and the “cutting” surface is possible. This is clearly illustrated in Fig. 3 where the intersection between the “cutting” surface and the second band surface gives rise to the wave-vector gap of band 2 in Fig. 27.

IV. METALLIC AND POLARITONIC PHOTONIC CRYSTALS IN 2D

Our first nontrivial illustration of the CSM introduced above is for a 2D photonic crystal made from metallic cylinders placed on a square lattice. The dielectric function of the metallic component is modeled by Eq. (3). Here we consider only the TM polarization (\vec{E} field is parallel to the cylinders). The optical properties of 2D photonic crystals with one metallic component have been the subject of various theoretical studies [6–9, 11, 37–41]. This interest in the 2D case was facilitated by the possibility of solving Eq. (1) using similar techniques to those used for FID’s provided that the 2D FDD has certain specific expressions for $\varepsilon(\omega)$.

We consider a photonic crystal consisting of metallic cylinders of radius $r = 0.472|a|$ placed in air on a square lattice of lattice constant $|a|$. The volume filling fraction of the cylinders is 0.7. Figure 1(b) of Ref. [7] displays the photonic band structure as calculated using a “modified plane wave method.” The plasma frequency in this case was chosen such that $\omega_p|a|/2\pi c = 1$ and the electric scattering time $\tau = \infty$ (c is the speed of light). Figure 5 illustrates the CSM construction of the photonic band structure of this photonic crystal. The lowest ten band surfaces corresponding to the Brillouin zone path Γ - M - X - Γ are shown together with the “cutting” surface defined by Eq. (3). The intersections of the band surfaces with the “cutting” surface projected onto the (\vec{k}_b, ω) plane, represent the photonic band structure of the FDD. Figure 6,

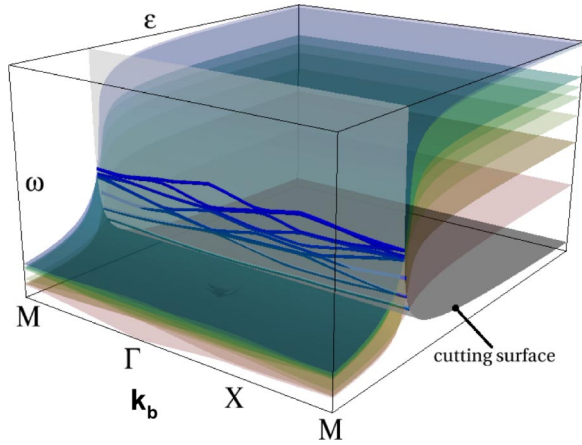


FIG. 5. (Color online) The band structure of a FDD consisting of metallic cylinders of radius $r=0.472|a|$ on a square lattice of lattice constant $|a|$ is calculated using the method introduced in Sec. III. The ten lowest TM (\vec{E} parallel to the cylinders) band surfaces corresponding to the Brillouin zone path Γ - M - X - Γ are “cut” with the surface defined by Eq. (3) where $\omega_p|a|/2\pi c=1$ and $\tau=\infty$. The intersections of the band surfaces with the “cutting” shape are also illustrated. ε runs from -30 to $+10$.

obtained by the CSM, accurately reproduces Fig. 1(b) of Ref. [7], obtained by more restrictive methods.

Using the intuitive construction shown in Fig. 5, we now consider the evolution of the photonic band structure as ω_p changes. When $\omega_p|a|/2\pi c$ decreases below 1 the intersections between the “cutting” surface and the band surfaces move toward larger ε values, implying an overall lowering of the band frequencies. When $\tau \neq \infty$ the “acoustic branch” of the photonic band structure is expected to appear eventually as the free carrier density (implicit in ω_p) is further reduced. An increase of $\omega_p|a|/2\pi c$ leads initially to upward movement of the bands’ frequencies. However, as a consequence of the flatness of the band surfaces in the negative ε area (clearly visible in Fig. 5) the lowest band becomes insensi-

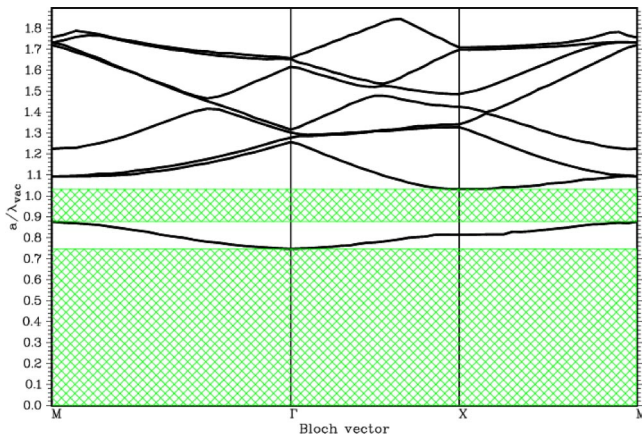


FIG. 6. (Color online) TM FDD photonic band structure of a photonic crystal which consists of metallic cylinders whose dielectric constant is given by Eq. (3) where $\omega_p|a|/2\pi c=1$ and $\tau=\infty$. The cylinders are placed on a square lattice of lattice constant $|a|$ and have a radius $r=0.472|a|$.

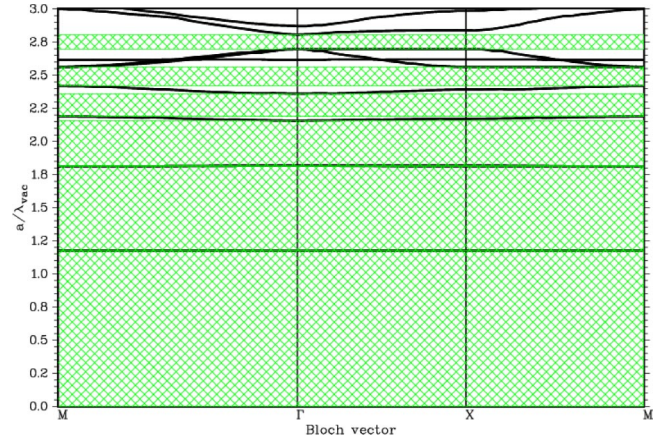


FIG. 7. (Color online) TM FDD photonic band structure for a metallic photonic crystal with the same geometry as the one described in the caption of Fig. 6, except with $\omega_p|a|/2\pi c=3$. The flat “pass bands” now appear below the plasma frequency.

tive to this increase in ω_p . This happens in turn to the higher bands. Figure 7 shows the TM photonic band structure obtained in the case $\omega_p|a|/2\pi c=3$. At low frequencies this photonic crystal remarkably behaves like a “photonic pass gap” material due to the presence of the flat photonic bands clearly visible for $\omega|a|/2\pi c \lesssim 2.5$ in Fig. 7. Here, the plasma gap that would normally appear for *all* frequencies below ω_p is now punctured by the presence of the narrow bands of propagating radiation. Physically, these flat bands describe EM modes in which the field energy is able to percolate through the “air” fraction of the photonic crystal and avoid significant concentration in the metal fraction. In the case of 3D metallic PBG materials, this type of band structure can have profound implications for blackbody radiation emitted from the interior of a 3D periodically structured metal such as tungsten [16]. In particular, it is possible to redistribute blackbody radiation from the frequency regions forbidden by the plasma gap into higher-frequency “photonic pass bands” for high-efficiency light filaments.

As another example we discuss the case of ionic crystals with polaritonic dielectric function. The dielectric constant in this case is given by the real part of Eq. (5). A typical plot of the real part of Eq. (5) (for small γ) is shown in Fig. 8. In the 2D case, this particular $\varepsilon(\omega)$ also facilitates a mapping of Eq. (1) to an ordinary eigenvalue problem [35,42,43]. Special geometries can also be treated in this case [44]. Figure 9 displays the TM band surfaces of a photonic crystal made from cylinders of radius $r=0.472|a|$ placed on a square lattice of radius $|a|$. The band surfaces (determined entirely by the geometrical structure of the photonic crystal) shown in Fig. 9 are identical with the ones displayed in Fig. 5. Before showing a specific numerical example of a photonic band structure for a particular choice of FDD parameters in Eq. (5), we discuss some of the important qualitative features that emerge in this case. In the limit $\gamma \rightarrow 0$, the dielectric function increases to arbitrary positive values as ω approaches ω_T from below and decreases to arbitrary negative values as it approaches ω_T from above (see Fig. 8). In these circumstances each band surface intersects the “cutting” surface three times, with two of the intersections (for positive ε)

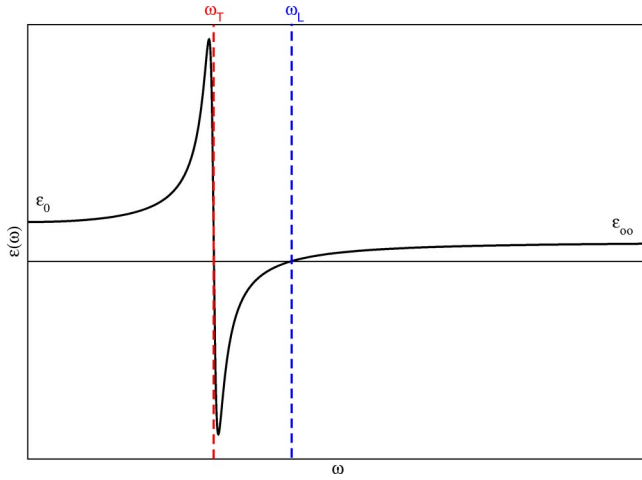


FIG. 8. (Color online) Real part of the polaritonic dielectric constant given by Eq. (5). The function is negative for $\omega_T < \omega < \omega_L$.

located close to ω_T . Because the frequency of any band is a monotonically decreasing function of ϵ , in the absence of damping an infinite number of “intersections” will accumulate around ω_T . This leads to a large accumulation of flat bands located around ω_T in the region where ϵ is positive. No such accumulation is expected for frequencies near or above ω_L . For $\omega \gg \omega_L$ the photonic bands quickly approach those of a FID photonic crystal with dielectric constant ϵ_∞ . The qualitative features described above are evident in Ref. [35] and are independently confirmed in Fig. 10 using the CSM. The TM photonic band structure shown in Fig. 10 corresponds to the following set of parameters: $\epsilon_0=12.66$, $\epsilon_\infty=10.9$, $\omega_T=0.4$, and $\gamma=0.01$. The accumulation of the bands just below $\omega=0.4$ is clearly evident. If ω_T and/or ω_L can be tuned, significant changes in the photonic band structure occur only in the region $\omega_T < \omega < \omega_L$ and the most sensitive area is near ω_T .

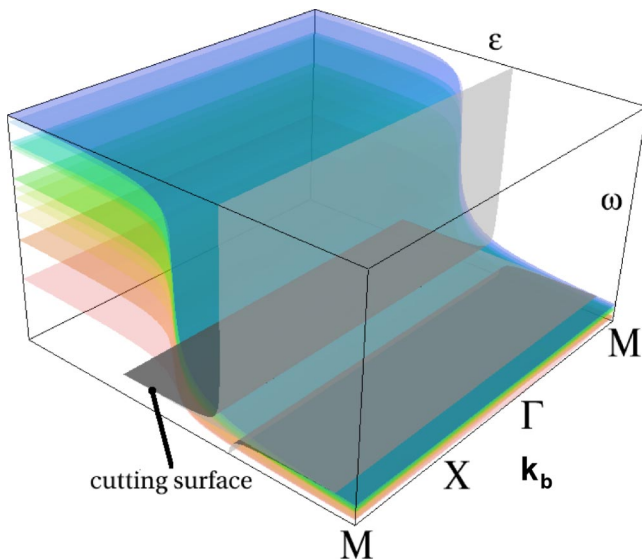


FIG. 9. (Color online) TM photonic band structure of a FDD crystal with a polaritonic resonance described by Eq. (5). The geometry of the crystal is identical with the one used in Fig. 5.

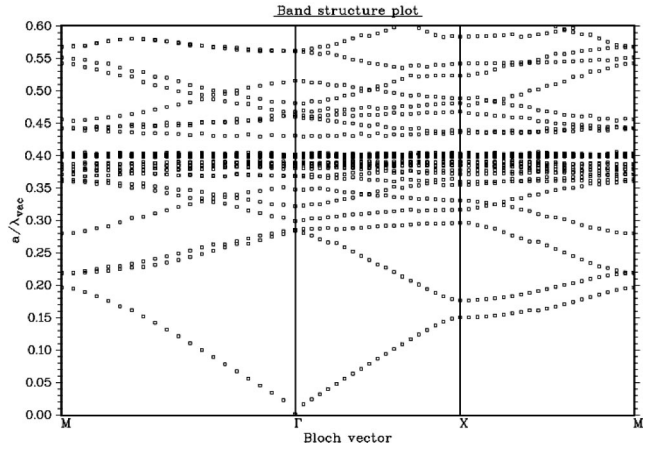


FIG. 10. TM photonic band structure for a polaritonic photonic crystal with solid cylinders of radius $0.472|a|$ on a square lattice of radius $|a|$. The cylinders are made from a polar crystal material whose dielectric constant is given by Eq. (5). The parameters used in this case are $\epsilon_0=12.66$, $\epsilon_\infty=10.9$, $\omega_T=0.4$, and $\gamma=0.01$.

Our calculation of the FDD photonic band structure using the CSM is based on initially obtaining a family of FID band structures, to generate the band surfaces. In this section we used the plane wave method [4] to perform these FID calculations. This method converges rapidly in the case of a positive dielectric constant. However, in the case of a negative dielectric constant its convergence can be reliably verified only in the case of a 2D TM field. In the case of a 2D TE field we find that the plane wave method performs well only when the volume filling fraction of the component with negative dielectric constant is small.

V. THREE-DIMENSIONAL PHOTONIC CRYSTALS

Unlike other specialized approaches to solving the photonic band structure of a FDD, the method introduced in Sec. III applies straightforwardly to three-dimensional photonic crystals. As a first example we consider the case of a close packed fcc crystal assembled from polystyrene spheres whose surfaces have been doped with an organic dye. This structure does not exhibit a 3D photonic band gap, but it does illustrate certain key concepts underlying FDD's in which a direct comparison between theory and experiment is already available. This particular type of photonic crystal has been studied in Ref. [24] where a large enhancement of a particular stop gap was reported due to the addition of the dye. Here, we present a model which interprets and explains this observation. The fcc lattice constant is denoted by $|a|$ and the close packed radius by $r_{cp}=|a|/2\sqrt{2}$. The polystyrene spheres are modeled as a spherical core of radius $0.9r_{cp}$ coated with a shell of thickness $\delta_{coating}=0.1r_{cp}$. The core is made from polystyrene and has a dielectric constant $\epsilon_{core}(\omega)=n_{core}^2=(1.592)^2$ which is frequency independent. For the coating we choose the frequency-dependent dielectric constant given by

$$\epsilon_{coating}(\omega) = \epsilon_0 + \Omega^2 \frac{\omega_0^2 - \omega^2}{(\omega_0^2 - \omega^2)^2 + \omega^2 \gamma_0^2} \quad (8)$$

where ϵ_0 , ω_0 , γ_0 , and Ω are numerical parameters. Equation (8) represents the real part of the dielectric constant of a

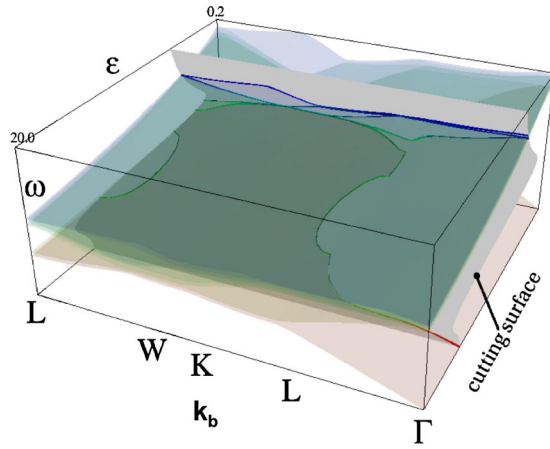


FIG. 11. (Color online) The “cutting” surface is defined by Eq. (8). The band surfaces correspond to a photonic crystal which consists of a fcc close packed arrangement of spheres whose surfaces have been infiltrated with an organic dye. We assume that the dye penetrated only a 10% radial distance inside the spheres. ϵ runs from 0.2 to 20.

material which includes a resonant component as well as other contributions to the dipole moment [45]:

$$\epsilon(\omega) = \epsilon_0 + \frac{4\pi N e^2}{m} \frac{f_0}{\omega_0^2 - \omega^2 - i\gamma_0\omega}$$

where f_0 is the fraction of the electrons in a molecule coupled resonantly at frequency ω_0 and ϵ_0 is the contribution to the dielectric from the rest of the electrons.

Figure 11 illustrates the construction of the band structure of the photonic crystal described above. The “cutting” surface is defined by Eq. (8) with the following parameters: $\epsilon_0=7$, $\omega_0=0.489$, $\gamma_0=0.3$, and $\Omega=\sqrt{1.9}$ (where all the frequencies are measured in units of $2\pi c/|a|$). Figure 12 shows the photonic band structure obtained by projecting the intersections between this “cutting” surface and the band surfaces on the (\vec{k}_b, ω) plane. The origin of the unusually shaped

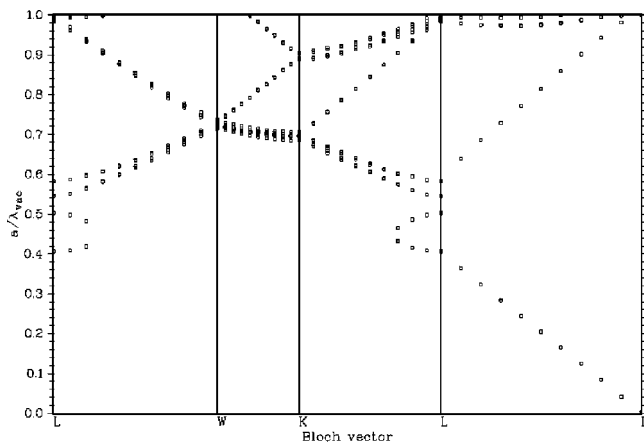


FIG. 12. FDD photonic band structure obtained by projecting the intersections between the “cutting” surface and the band surfaces shown in Fig. 11. A large stop gap (see Fig. 13) opens in the Γ - L direction.

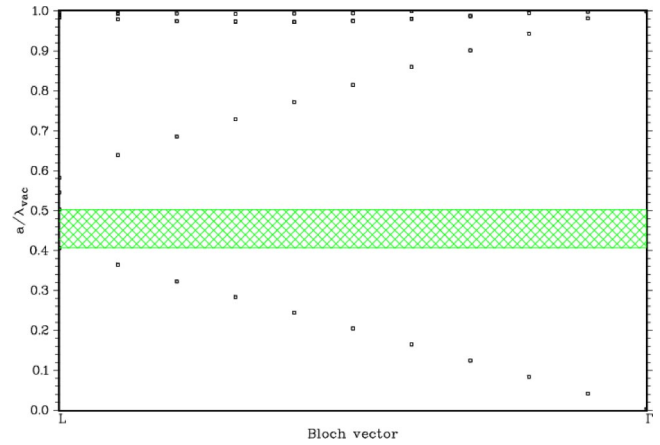


FIG. 13. (Color online) A section of the photonic band structure displayed in Fig. 12 which illustrates the stop gap in the Γ - L direction. The relative size of the stop gap ($>20\%$) is much bigger than the one obtained in the absence of the dispersion and is entirely attributed to the placement of the “cutting” surface relative to the band surfaces in Fig. 11. See also Fig. 14.

bands (wave-vector gap) near the L point can be understood from the graphical solution displayed in Fig. 11. We also note the significant increase of the Γ - L stop gap illustrated in Fig. 13. This occurs because the edges of the stop gap are located at different ϵ values. Figure 14 illustrates the formation of the band frequencies at the L point. The dashed curves represent the frequency of the lowest two bands (which are doubly degenerate in this case) at the L point as calculated with a frequency-independent method. The continuous curve is defined by Eq. (8) (the functional inverse to be more precise). As seen in the figure there are four intersections generated by these two bands and the “cutting” curve. These points are also visible in Fig. 12 or Fig. 13. The

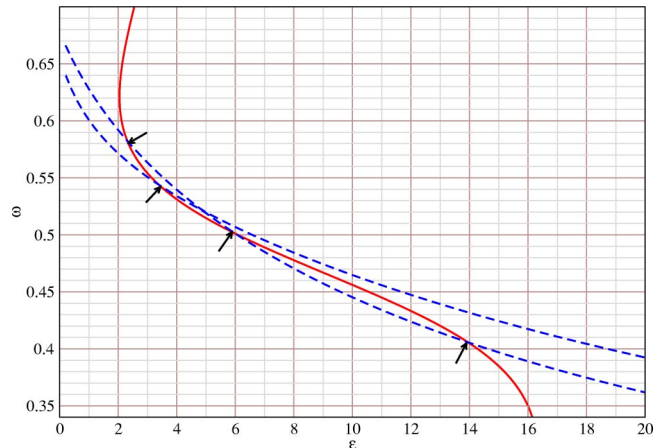


FIG. 14. (Color online) Graphical solution for the calculation of the lowest four frequencies at L point for the system discussed in Fig. 11. The dashed curves represent the frequencies of the lowest two bands as a function of ϵ as calculated with a frequency-independent method. The continuous curve represents Eq. (8) used to define the “cutting” surface in Fig. 11. The four intersections correspond to the lowest four frequencies at the L point in Fig. 12 or Fig. 13.

apparent stop gap (as measured by reflectivity) at the L point is dramatically stretched to about 20% of the center frequency. In the absence of the dye molecules, this stop gap would be below 1%.

The construction displayed in Fig. 14 is general and suggests that band gaps (full or partial) can always be increased around the area of anomalous dispersion ($\text{Re}[\varepsilon(\omega)]$ decreases with ω). This occurs because the lower edge is pushed toward larger ε values (which also implies lower frequencies) whereas the upper edge is pulled toward lower ε values (higher frequencies). Due to a scarcity of experimental parameters given in Ref. [24], we used a generic set of parameters for the dielectric function in Eq. (8). The parameters were chosen based on plausibility to match the observed enlargement of the photonic stop gap. Of crucial importance in this case is the “matching” between the natural frequency of the resonators and the geometry of the crystal. As this and the remaining examples show, only carefully engineered photonic crystals (with appropriate placement of resonators in both frequency and spatial location) can take full advantage of the potential to mold the PBG offered by the frequency-dependent dielectrics.

As a second example of a 3D FDD, we consider the inverted opal consisting of a collection of resonators. We again describe the resonator component using Eq. (8). The photonic crystal consists of an assembly of spherical shells placed on a fcc lattice of lattice constant $|a|$. Each spherical shell is modeled as an air spherical core of radius $|a|/2\sqrt{2}$ (fcc close packed radius) coated with a solid shell of thickness $\delta_{\text{coating}}=0.08|a|$. This corresponds to approximately 25% volume fraction of the solid component. Everywhere except the solid shell, the dielectric constant is 1. A possible realization of this model consists of densely packed PbS or PbSe colloidal quantum dots embedded in a suitable polymer matrix. First we illustrate the photonic band gap enhancement effect suggested above. Figure 15 shows the photonic band structure of this FDD obtained by using Eq. (8) with the following parameters: $\varepsilon_0=12$, $\Omega=\sqrt{2}$, $\omega_0=0.82$, and $\gamma_0=0.3$. The parameters used here are chosen such that the full photonic band gap is more than double the size of an inverted opal photonic crystal made from a material with a frequency-independent dielectric constant with $\varepsilon=12$.

The most important parameter determining the character of the photonic band structure is ω_0 . Changing the resonant frequency ω_0 from 0.82 to 0.675 results in the combination of band surfaces and “cutting” surface displayed in Fig. 16. The projections of the intersections shown in Fig. 16 on the (\vec{k}_b, ω) plane and the FDD photonic band structure are shown in Fig. 17. Here, we note the appearance of a set of unusually shaped photonic bands. The closed curves appearing above the fourth band surface have their origin in the intersection between a single band surface and the “cutting” surface (see Fig. 16). These “dispersion bubbles,” accompanied by wave-vector gaps, maintain the same character along their contour (dielectric or air band) and span a spectral region in which the FDD component of the photonic crystal exhibits anomalous dispersion. Accordingly, the imaginary part of the dielectric constant is crucial in interpreting their physical consequences.

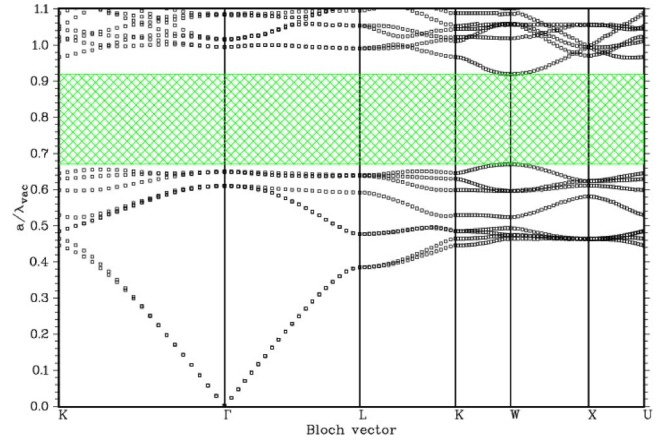


FIG. 15. (Color online) Photonic band structure corresponding to a FDD inverted opal of core radius $|a|/2\sqrt{2}$ and $\delta_{\text{coating}}=0.08|a|$ where $|a|$ is the fcc lattice constant. The frequency dependence of the solid material consisting of a dense collection of noninteracting resonators (the shell of thickness δ_{coating}) is given by Eq. (8) where the following parameters have been used: $\varepsilon_0=12$, $\Omega=\sqrt{2}$, $\omega_0=0.820$, and $\gamma_0=0.3$. ω_0 was chosen such that the dielectric “cutting” surface intersects the lower and upper bands at widely separated ε values, thus pushing apart the two band edges.

VI. ANALYSIS OF WAVE-VECTOR GAP REGIONS

In this section we focus our attention on the spectral region around a “dispersion bubble” where a WVG occurs. As a concrete example we use a 1D photonic crystal characterized by $[n_1, |d|_1]=[\sqrt{\varepsilon(\omega_s)}, 0.2|a|]$ and $[n_2, |d|_2]=[1, 0.8|a|]$ where $\varepsilon(\omega_s)$ is defined by

$$\varepsilon(\omega_s) = \varepsilon_0 + \Omega^2 \frac{1}{\omega_0^2 - \omega_s^2 - i\gamma\omega_s} \quad (9)$$

with $\varepsilon_0=12$, $\Omega=2$, $\omega_0=0.88$, and $\gamma=0.35$. The FDD photonic band structure of this crystal [obtained from the real part

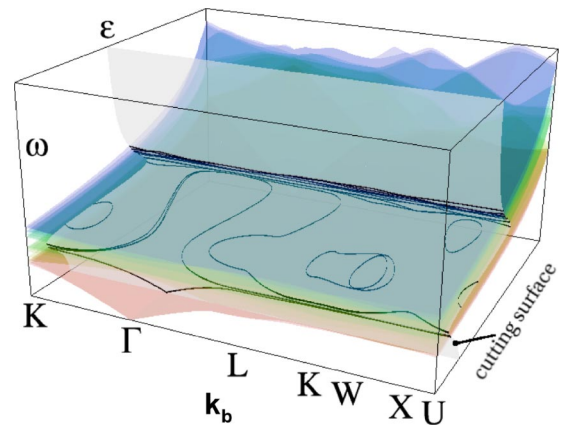


FIG. 16. (Color online) The “cutting” surface is defined by Eq. (8) with the following parameters: $\varepsilon_0=12$, $\Omega=\sqrt{2}$, $\omega_0=0.675$, and $\gamma_0=0.3$. The band surfaces correspond to an inverted opal of core radius $|a|/2\sqrt{2}$ and $\delta_{\text{coating}}=0.08|a|$ where $|a|$ is the fcc lattice constant. The “islands” created by the intersection between a single band surface and the “cutting” surface give rise to the “closed” bands in the photonic band structure displayed in Fig. 17 above the fourth band.

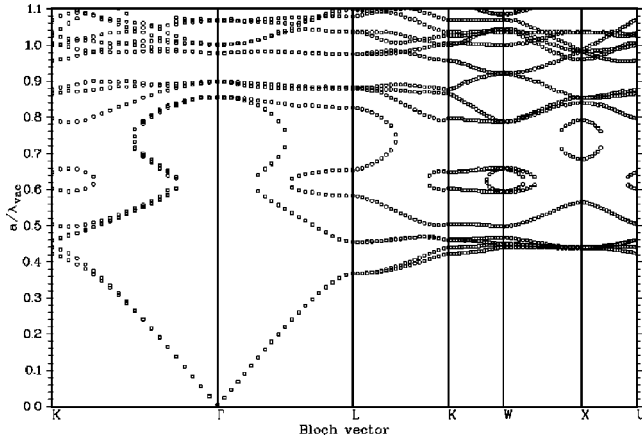


FIG. 17. Photonic band structure obtained by projecting the intersections shown in Fig. 16 on the (\vec{k}_b, ω) plane.

of Eq. (9) is shown in Fig. 18. As illustrated in Fig. 19, the “turning” band, which extends from approximately 0.88 to 1.08, is placed entirely on the abnormal region of the dispersion relation (defined as the spectral region in which $d\text{Re}[\varepsilon(\omega)]/d\omega < 0$). The striking feature of this particular band is the fact that around $\omega_s \approx 0.965$ $|\nabla_{\vec{k}_b} \omega(\vec{k}_b)|$ becomes infinite. However, an infinite slope in the frequency dispersion relation does not directly imply an infinite speed for the propagation of electromagnetic energy as this connection is valid only in the case of smooth frequency dispersion relations [45]. Theoretical and experimental studies of pulses tunneling or propagating through media which exhibit anomalous dielectric dispersion are numerous [46–48]. Here we analyze the combined effect of an anomalous dielectric dispersion together with the existence of an infinite slope in the frequency dispersion.

To this end we study the propagation of a pulse with a finite duration through a finite 1D photonic crystal which consists of ten unit cells described in the caption of Fig. 18.

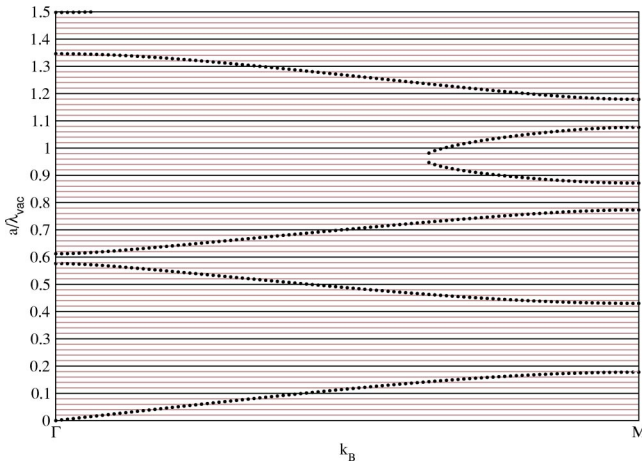


FIG. 18. FDD photonic band structure which exhibits a dispersion bubble at frequencies around $\omega|a|/2\pi c = 0.965$. The crystal is characterized by $[n_1, |d_1|] = [\text{Re}[\sqrt{\varepsilon(\omega_s)}], 0.2|a|]$ and $[n_2, |d_2|] = [1, 0.8|a|]$ where $\varepsilon(\omega_s)$ is defined by Eq. (9) with $\varepsilon_0 = 12$, $\Omega = 2$, $\omega_0 = 0.88$, and $\gamma = 0.35$.

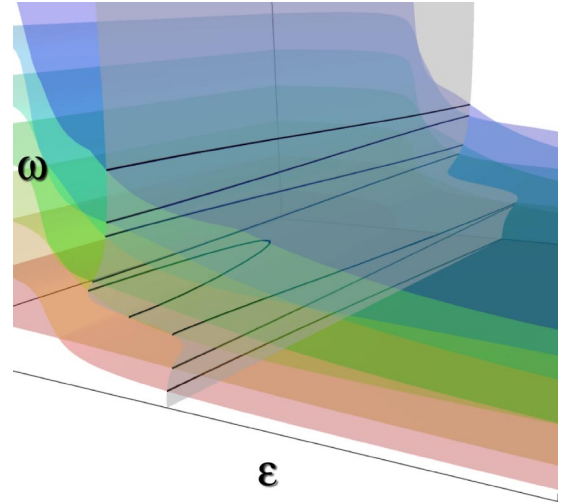


FIG. 19. (Color online) The first six band surfaces and the intersections with the “cutting” surface defined by Eq. (9) with $\varepsilon_0 = 12$, $\Omega = 2$, $\omega_0 = 0.88$, and $\gamma = 0.35$. The band surfaces correspond to the 1D photonic crystal described in the caption of Fig. 18.

Figure 20 displays the configuration used in the simulation. For plane waves incident on the photonic crystal from the left one has the following expressions for the field to the left of x_A , E_l , and to the right or x_B , E_r :

$$E_l(x, t) = e^{-i\omega t + i\omega/c(x-x_A)} + R(\omega)e^{-i\omega t - i\omega/c(x-x_A)},$$

$$E_r(x, t) = T(\omega)e^{-i\omega t + i\omega/c(x-x_B)},$$

where T and R are the transmission and reflection coefficients which can easily be calculated for any 1D photonic crystal using a boundary matching transfer matrix approach. In order to simplify the notation we choose the speed of light to be 1 from now on. We assume that at x_S the time profile of the incoming pulse is given by

$$E_{\text{in}}(x_S, t) = e^{-i\omega_c t} \mathcal{E}(t)$$

where ω_c is the center frequency of the pulse and $\mathcal{E}(t)$ is an envelope function which vanishes outside the time interval $[-\Delta\tau/2, \Delta\tau/2]$:

$$\mathcal{E}(t) = \begin{cases} 0 & \text{for } |t| \geq \Delta\tau/2, \\ \frac{(\Delta\tau^2 - 4t^2)^7}{\Delta\tau^{14}} & \text{for } |t| \leq \Delta\tau/2. \end{cases} \quad (10)$$

In our simulation we use $\Delta\tau = 400$, $x_S = -200|a|$, and $x_D = x_B$. The clock is set such that the input pulse reaches its maximum at position x_S at $t = 0$. Figure 21 displays the absolute value of the amplitude of the input pulse as measured at x_S . It can be shown that the output pulse is written as

$$E_{\text{out}}(x_D = x_B, t) = \int_{-\infty}^{\infty} d\omega F(\omega) T(\omega) e^{-i\omega t} \quad (11)$$

where $F(\omega)$ is the Fourier transform of the input pulse and $T(\omega)$ is the transmission coefficient through the finite photonic crystal. We first study pulse propagation assuming that the dielectric function is real and neglect completely the

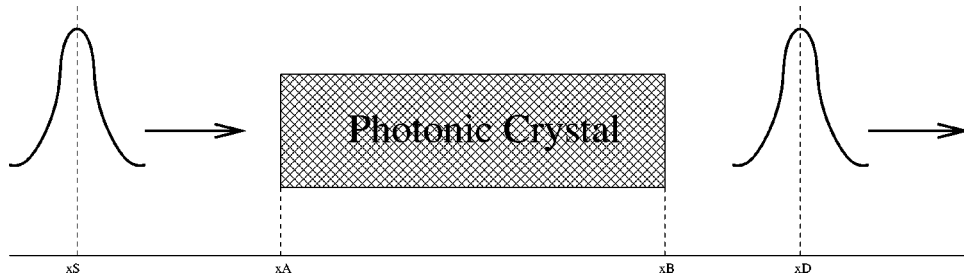


FIG. 20. The setup used for studying the propagation of a pulse through a 1D photonic crystal. The photonic crystal extends from x_A to x_B . The source pulse is given at position x_S and the outgoing pulse is detected at position x_D . The photonic crystal is completely characterized by transmission and reflection coefficients T and R , respectively.

imaginary part of Eq. 9 in the calculation of $T(\omega)$. By doing so we obtain the output pulse (time profile measured at x_B) displayed in Fig. 22. The pulse is centered at frequency $\omega|a|/2\pi c=0.90$ which falls on the anomalous region of $\epsilon(\omega)$. The peak of the input pulse reaches the photonic crystal at $t=200$. In vacuum, the peak of the pulse is expected to reach x_B (the end of the photonic crystal) at $t=210$. In the presence of the photonic crystal we find that the peak of the pulse emerges from the photonic crystal at $t=184$. As we will see later, the peak of the pulse cannot be used as a good marker for the measurement of the transit time, therefore we disregard for now the apparent superluminal transport suggested by the tracking of the peak. However, in this case we find the front of the peak to exhibit noncausal behavior. At $t=0$ the front of the pulse just reaches the left boundary (x_A in Fig. 20) of the photonic crystal. Therefore causality implies that for $t \leq 0$ the pulse measured at x_B will be 0 as well. The time profile of the output pulse as predicted by Eq. (11) at x_B shows that in fact the intensity is not zero even for $t < 0$. The output pulse has been calculated numerically with high accuracy and the values obtained at $t < 0$, although invisible on the scale of Fig. 22, are above the numerical error used in calculations.

The unphysical prediction of noncausal propagation near a WVG is due to the fact that in the calculations we have neglected completely the imaginary part of the dielectric

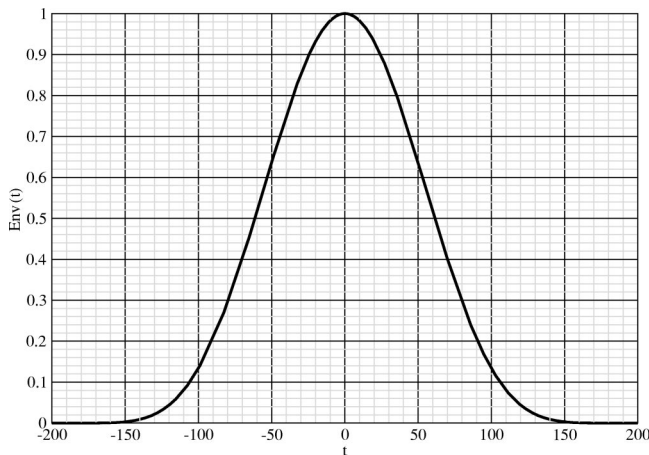


FIG. 21. The absolute value of the amplitude of the input pulse as measured at x_S (see Fig. 20). This is a plot of the envelope function given by Eq. (10) for $\Delta\tau=400$.

constant. As is well known, the imaginary part of the dielectric constant plays a crucial role in maintaining causality of field equations. The Kramers-Kronig relations [45], which stem from the causality connection between \vec{D}_ω and \vec{E}_ω , require the presence of the imaginary part for a dielectric constant such as the one used in Eq. (9). Figure 23 displays the absolute value of the transmission coefficient through the same 1D finite photonic crystal described above. We use the complex form of the dielectric constant [Eq. (9)]. Due to the relatively large imaginary part present in this case we see a low transmission around $\omega|a|/2\pi c=0.90$. Figure 24 displays the time profile of the output pulse as measured at position x_B (see Fig. 20). The amplitude of the output pulse is clearly reduced but the shape of the pulse is almost unchanged. Here we also see that the peak of the output pulse emerges from the photonic crystal before the peak of the input pulse reaches the entry of the photonic crystal. However, in sharp distinction to the case in which the imaginary part of the dielectric constant was neglected, we now find that for $t \leq 0$ there is no output, as required.

The fact that the peak of the pulse emerges from the photonic crystal before it enters is not a violation of causality.

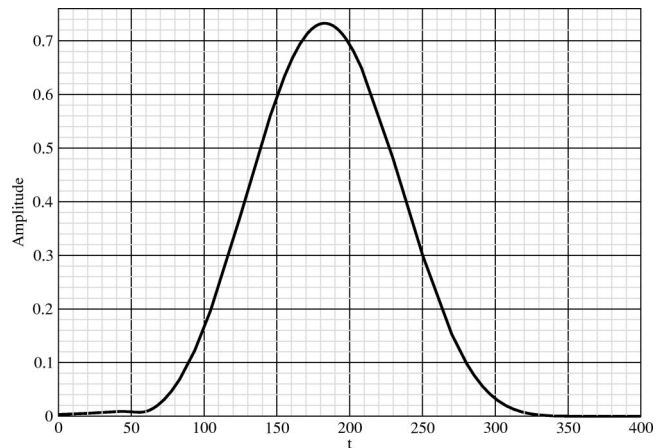


FIG. 22. The input pulse whose intensity profile is shown in Fig. 21 passes through a 1D photonic crystal made from ten unit cells described in the caption of Fig. 18. The pulse is centered at frequency $\omega|a|/2\pi c=0.90$. The peak of the input pulse reaches the photonic crystal at $t=200$ and emerges at x_B at $t=184$. This plot shows the absolute value of the amplitude of the output pulse as measured at x_B . In the calculation the imaginary part of Eq. (9) was neglected.

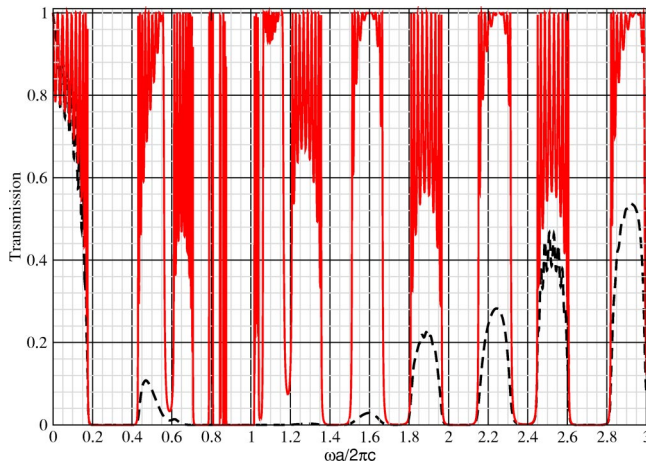


FIG. 23. (Color online) Dashed (black) line, the absolute value of the transmission coefficient of the 1D photonic crystal made from ten unit cells whose characteristics are described in the caption of Fig. 18. The imaginary part of $\varepsilon(\omega)$ was kept in the calculation. Solid (red) line, the transmission coefficient for the unphysical case in which the imaginary part of $\varepsilon(\omega)$ was neglected.

Consider for example an input pulse in vacuum which, at a certain position x_D , exhibits the time profile displayed as a dashed line in Fig. 25. The peak of this pulse reaches x_D at time t_1 and has amplitude A_1 . Suppose that after the input pulse passes through the medium (photonic crystal or a medium which exhibits anomalous dispersion) the output pulse measured at the same position has the time profile shown as filled in Fig. 25. The peak of this new pulse reaches x_D at time $t_2 < t_1$ and has an amplitude $A_2 < A_1$. This illustrates that the peak of the pulse cannot be used as a “marker” for the speed with which information propagates.

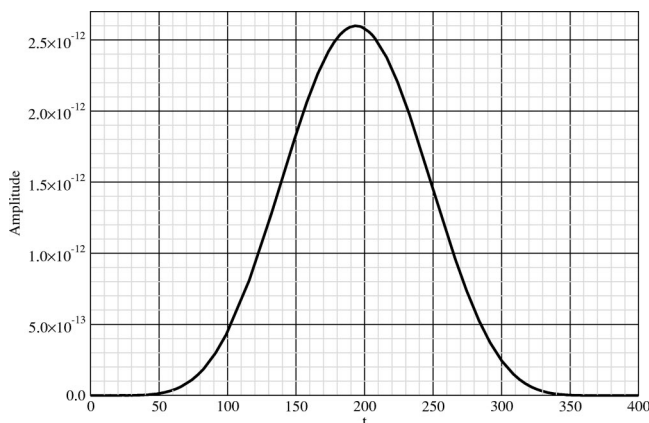


FIG. 24. The same finite photonic crystal and input pulse as in the case described in the caption of Fig. 22. The difference in this case is the fact that in the calculation of the output pulse the imaginary part of Eq. (9) is not neglected. In this case the amplitude of the emerging pulse is greatly reduced and the peak of the pulse is also seen to exit the photonic crystal before it enters. The intensity of the output pulse is 0 for $t < 0$.

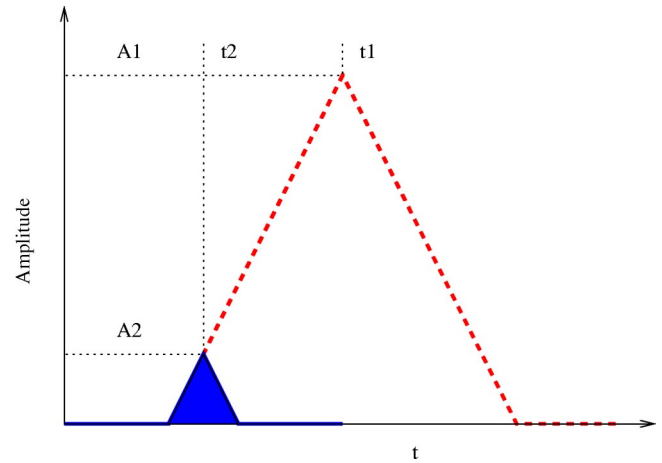


FIG. 25. (Color online) Superluminal propagation? The dashed curve shows the output pulse after passing through vacuum. The filled pulse shows a fraction of the whole pulse. The peak of the whole pulse has amplitude A_1 and occurs at time t_1 . The peak of the fraction pulse is $A_2 < A_1$ and occurs at $t_2 < t_1$.

VII. SUMMARY

We have presented a general method for calculating the photonic band structure of photonic crystals with a frequency-dependent dielectric constant. The method applies equally well to 1D, 2D, and 3D structures. We find excellent agreement with an exact 1D model and previously published results on some special 2D cases. The flexibility and predictive power of our method were illustrated with a few 2D and 3D examples. We showed how the photonic band gap in the presence of a frequency-dependent dielectric can be enhanced by a careful match between the geometry of the structure and electronic properties (such as resonant frequency) of the frequency-dependent material. While already extremely powerful, the method presented here can be further improved by addressing its current limitations: (i) the method does not treat (in a computationally efficient manner) photonic crystals with more than one FDD component, and (ii) the method does not treat dielectric constants with both a real and imaginary part.

ACKNOWLEDGMENTS

This work was supported in part by the Natural Sciences and Engineering Research Council of Canada and a grant from William F. McLean.

APPENDIX: PHOTONIC BAND STRUCTURE OF A 1D PHOTONIC CRYSTAL

The simplest illustration of a photonic crystal band structure is provided by the multilayered structure consisting of an alternating sequence of two materials. The unit cell has a

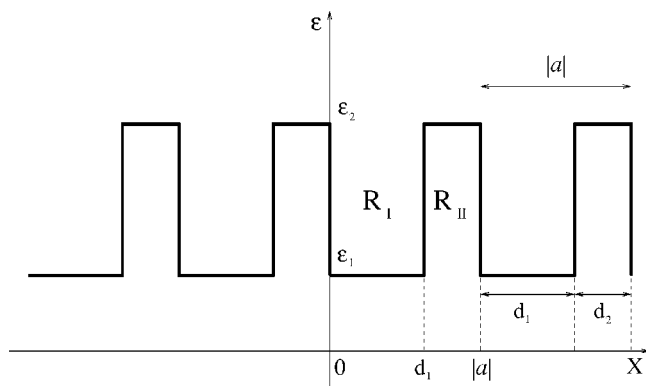


FIG. 26. Spatial profile of the dielectric constant in a 1D photonic crystal. The lattice constant is $|a|$ and the two components are characterized by [dielectric, thickness] of $[\varepsilon_1, d_1]$ and $[\varepsilon_2, d_2]$, respectively.

thickness $|a|$ and the two components are characterized by [dielectric, thickness] of $[\varepsilon_1, d_1]$ and $[\varepsilon_2, d_2]$, respectively (we assume that the magnetic permeability μ is equal to unity in both components) (see Fig. 26). In the following we study only the behavior of electromagnetic waves of well defined real frequency ω propagating perpendicular to the layers:

$$\vec{E}(x, t) = E(x, t)\hat{z} = \vec{E}_\omega(x)e^{i\omega t}\hat{z}. \quad (\text{A1})$$

The equation satisfied by the field is

$$\frac{\partial^2 \vec{E}_\omega(x)}{\partial x^2} = -\frac{\omega^2 \varepsilon(x, \omega)}{c^2} \vec{E}_\omega(x). \quad (\text{A2})$$

Here we do not make any assumption about the frequency dependence of the dielectric constant. The index of refraction is defined by $n(x, \omega) \equiv \sqrt{\varepsilon(x, \omega)}$. We denote by n_1 and n_2 the indices of refraction of the two components, respectively, and drop the ω dependence of both n_1 and n_2 in the expressions below. We also note that the index of refraction can be imaginary in a region where the dielectric constant is negative.

Due to the spatial periodicity of the dielectric constant, the solution of Eq. (A2) can be written as [49]

$$\vec{E}_\omega(x) = e^{i\mathbf{k}_b x} \mathcal{E}_\omega(x) \quad (\text{A3})$$

where \mathbf{k}_b is the Bloch vector and \mathcal{E}_ω is the Bloch function. \mathbf{k}_b is restricted to the first Brillouin zone which in the 1D case corresponds to $-\pi/|a| \leq \mathbf{k}_b \leq \pi/|a|$. The Bloch function satisfies the periodicity condition

$$\mathcal{E}_\omega(x) = \mathcal{E}_\omega(x + a) \quad \forall x. \quad (\text{A4})$$

With the notation $k_0 \equiv \omega/c$, by making use of Eq. (A3), Eq. (A4), and the continuity of the solution, one finds the following relation between the Bloch vector and the frequency of the mode [49]:

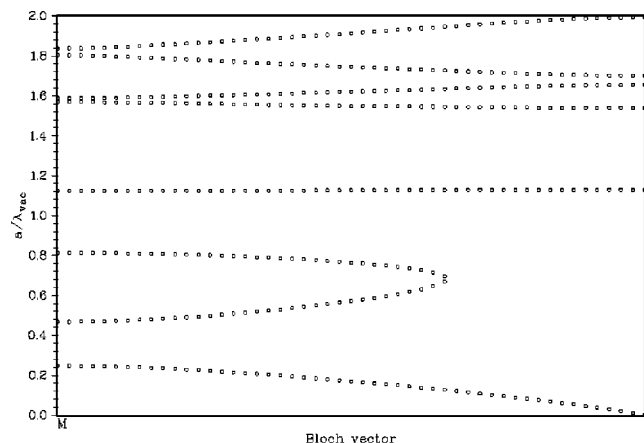


FIG. 27. Band structure of a 1D photonic crystal made from alternating layers characterized by $\varepsilon_1(\omega_s) = 10 \sin(4\omega_s)$, $\varepsilon_2 = 1$, and $d_1/|a| = 0.2$. The frequencies are calculated using Eq. (A5) and ω_s is defined in Eq. (A6). \mathbf{k}_b runs from 0 at Γ to $\pi/|a|$ at M .

$$\begin{aligned} \cos(\mathbf{k}_b a) &= \cos(k_0 n_1 d_1) \cos(k_0 n_2 d_2) \\ &\quad - \frac{n_1^2 + n_2^2}{2n_1 n_2} \sin(k_0 n_1 d_1) \sin(k_0 n_2 d_2). \end{aligned} \quad (\text{A5})$$

In the following we will take $n_2(\omega) = 1$ and $n_1(\omega) = \sqrt{\varepsilon(\omega)}$. In order to simplify the notation we measure the distances in units of $|a|$ and \mathbf{k}_b in units of $|a|^{-1}$. The frequency is measured in units of $2\pi c/|a|$ by the introduction of the scaled frequency ω_s , defined by

$$\omega_s \equiv \frac{v_s}{2\pi} = \frac{k_0 |a|}{2\pi} = \frac{\omega |a|}{2\pi c} = \frac{|a|}{\lambda_{\text{vac}}}, \quad (\text{A6})$$

where λ_{vac} denotes the wavelength in vacuum. We note that Eq. (A5) contains only real terms for both positive and negative $\varepsilon(\omega_s)$.

For a given Bloch vector \mathbf{k}_b , Eq. (A5) is satisfied only for a set of frequencies ω_s (equivalently v_s) which represent the frequencies of the photonic bands at that particular Bloch vector. The solution of the transcendental Eq. (A5) completely determines the photonic band structure of the 1D photonic crystal. As an example we show in Fig. 27 the 1D photonic band structure obtained for a photonic crystal characterized by $d_1/|a| = 0.2$ (see Fig. 26), $\varepsilon_1(\omega_s) = 10 \sin(4\omega_s)$, and $\varepsilon_2 = 1$. The frequency dependence of the first layer's dielectric constant has no physical significance and was chosen just as an example.

This simple one-dimensional model exhibits features that are shared by all the photonic crystals in general. For example, the dispersion of the lowest band (also called the acoustic branch of the band structure by analogy with the propagation of elastic waves) at small \mathbf{k}_b is almost linear, which indicates that at long wavelengths the photonic crystal looks very much like a homogeneous medium for the propagating electromagnetic waves [50]. However, the presence of the acoustic band in the photonic band structure is not automatically guaranteed. If components with negative dielectric constant are present in the photonic crystal then the acoustic

branch can disappear (a cutoff frequency will appear at the Γ point). In the case of 1D photonic crystals we can calculate the exact conditions under which this cutoff appears.

$\mathbf{k}_b=0$, $k_0=0$ is always a solution of Eq. (A5). By neglecting the frequency dependence of ε_1 and ε_2 for $\omega \approx 0$ then for small deviations from 0 of both \mathbf{k}_b and k_0 we can approximate Eq. (A5) very well by

$$1 - \frac{(\mathbf{k}_b a)^2}{2} = 1 - \frac{1}{2} [(\varepsilon_1 + \varepsilon_2)d_1 d_2 + \varepsilon_1 d_1^2 + \varepsilon_2 d_2^2] k_0^2. \quad (\text{A7})$$

When $(\varepsilon_1 + \varepsilon_2)d_1 d_2 + \varepsilon_1 d_1^2 + \varepsilon_2 d_2^2 > 0$ Eq. (A7) gives a linear relation between \mathbf{k}_b and k_0 :

$$\mathbf{k}_b = \bar{n} \frac{\omega}{c}, \quad (\text{A8})$$

$$\bar{n}^2 = (\varepsilon_1 + \varepsilon_2) \frac{d_1 d_2}{a^2} + \varepsilon_1 \left(\frac{d_1}{a} \right)^2 + \varepsilon_2 \left(\frac{d_2}{a} \right)^2, \quad (\text{A9})$$

where \bar{n} is the effective index of refraction of the photonic crystal. \bar{n} is a bounded quantity so that the assumption made in approximating Eq. (A5) by Eq. (A7) is valid.

When $(\varepsilon_1 + \varepsilon_2)d_1 d_2 + \varepsilon_1 d_1^2 + \varepsilon_2 d_2^2 \leq 0$ Eq. (A7) cannot be satisfied for small, real, k_0 , hence the acoustic branch will disappear. For a 1D photonic crystal with $\varepsilon_2=1$ this condition is equivalent to

$$\varepsilon_1 < -\frac{1-d_1}{d_1}, \quad (\text{A10})$$

which shows that the greater the filling fraction of the negative epsilon component d_1 , the smaller the required threshold for the occurrence of the cutoff at Γ point. This feature of the photonic band structure is present in higher dimensions as well and is important for FDD photonic band structure calculations.

-
- [1] Sajeev John, Phys. Rev. Lett. **58**, 2486 (1987).
 [2] Eli Yablonovitch, Phys. Rev. Lett. **58**, 2059 (1987).
 [3] Sajeev John, Phys. Rev. Lett. **53**, 2169 (1984).
 [4] K. M. Ho, C. T. Chan, and C. M. Soukoulis, Phys. Rev. Lett. **65**, 3152 (1990).
 [5] Neil W. Ashcroft and N. David Mermin, *Solid State Physics* (Saunders College Publishers, Philadelphia, PA, 1976).
 [6] Arthur R. McGurn and Alexei A. Maradudin, Phys. Rev. B **48**, 17 576 (1993).
 [7] V. Kuzmiak, A. A. Maradudin, and F. Pincemin, Phys. Rev. B **50**, 16 835 (1994).
 [8] V. Kuzmiak and A. A. Maradudin, Phys. Rev. B **55**, 7427 (1997).
 [9] Vladimir Kuzmiak and Alexei A. Maradudin, Phys. Rev. B **58**, 7230 (1998).
 [10] Kazuaki Sakoda and Jun Kawamata, Opt. Express **3**, 12 (1998).
 [11] Kazuaki Sakoda, Noriko Kawai, Takunori Ito, Alongkarn Chutinan, Susumu Noda, Tsuneo Mitsuyuu, and Kazuyuki Hirao, Phys. Rev. B **64**, 045116 (2001).
 [12] Takunori Ito and Kazuaki Sakoda, Phys. Rev. B **64**, 045117 (2001).
 [13] J. B. Pendry and A. MacKinnon, Phys. Rev. Lett. **69**, 2772 (1992).
 [14] A. J. Ward, J. B. Pendry, and W. J. Stewart, J. Phys.: Condens. Matter **7**, 2217 (1995).
 [15] J. B. Pendry, J. Phys.: Condens. Matter **8**, 1085 (1996).
 [16] J. G. Fleming, S. Y. Lin, I. El-kady, R. Biswas, and K. M. Ho, Nature (London) **417**, 52 (2002).
 [17] U. Grüning, V. Lehmann, and C. M. Engelhardt, Appl. Phys. Lett. **66**, 3254 (1995).
 [18] S. Ottow, V. Lehmann, and H. Föll, Appl. Phys. A: Mater. Sci. Process. **63**, 153 (1996).
 [19] U. Grüning, V. Lehmann, S. Ottow, and K. Busch, Appl. Phys. Lett. **68**, 747 (1996).
 [20] S. W. Leonard, H. M. van Driel, J. Schilling, and R. B. Wehrspohn, Phys. Rev. B **66**, 161102(R) (2002).
 [21] A. A. Krokhin and P. Halevi, Phys. Rev. B **53**, 1205 (1996).
 [22] P. Halevi and F. Ramos-Mendieta, Phys. Rev. Lett. **85**, 1875 (2000).
 [23] Alvaro Blanco *et al.*, Nature (London) **405**, 437 (2000).
 [24] Sang Hyun Park, Byron Gates, and Younan Xia, Adv. Mater. (Weinheim, Ger.) **11**, 462 (1999).
 [25] A. Femius Koenderink, Lydia Bechger, H. P. Schriemer, Ad Lagendijk, and Willem L. Vos, Phys. Rev. Lett. **88**, 143903 (2002).
 [26] Sajeev John and Jian Wang, Phys. Rev. Lett. **64**, 2418 (1990).
 [27] John D. Joannopoulos, Robert D. Meade, and Joshua N. Winn, *Photonic Crystals* (Princeton University Press, Princeton, NJ, 1995).
 [28] M. A. Ordal, L. L. Long, R. J. Bell, S. E. Bell, R. R. Bell, R. W. Alexander, Jr., and C. A. Ward, Appl. Opt. **22**, 1099 (1983).
 [29] Charles Kittel, *Introduction to Solid State Physics*, 7th ed. (John Wiley & Sons, New York, 1996).
 [30] R. D. Meade, A. M. Rappe, K. D. Brommer, J. D. Joannopoulos, and O. L. Altherhand, Phys. Rev. B **48**, 8434 (1993).
 [31] Alexander Moroz, Phys. Rev. Lett. **83**, 5274 (1999).
 [32] W. Kohn and N. Rostoker, Phys. Rev. **94**, 1111 (1954).
 [33] W. M. Lee, P. M. Hui, and D. Stroud, Phys. Rev. B **51**, 8634 (1995).
 [34] Chul-Sik Kee and H. Lim, Phys. Rev. B **64**, 121103(R) (2001).
 [35] V. Kuzmiak, A. A. Maradudin, and A. R. McGurn, Phys. Rev. B **55**, 4298 (1997).
 [36] Weiy Zhang, An Hu, Xinya Lei, Ning Xu, and Naiben Ming, Phys. Rev. B **54**, 10 280 (1996).
 [37] Toshio Suzuki and Paul K. L. Yu, Opt. Lett. **20**, 2520 (1995).
 [38] Shanhuai Fan, Pierre R. Villeneuve, and J. D. Joannopoulos, Phys. Rev. B **54**, 11 245 (1996).
 [39] J. Arriaga, A. J. Ward, and J. B. Pendry, Phys. Rev. B **59**,

- 1874 (1999).
- [40] V. Yannopoulos, A. Modinos, and N. Stefanou, *Phys. Rev. B* **60**, 5359 (1999).
- [41] Esteban Moreno, Daniel Erni, and Christian Hafner, *Phys. Rev. B* **65**, 155120 (2002).
- [42] M. Sigalas, C. M. Soukoulis, E. N. Economou, C. T. Chan, and K. M. Ho, *Phys. Rev. B* **48**, 14 121 (1993).
- [43] M. M. Sigalas, C. M. Soukoulis, C. T. Chan, and K. M. Ho, *Phys. Rev. B* **49**, 11 080 (1994).
- [44] Kerwyn Casey Huang, Peter Bienstman, John D. Joannopoulos, Keith A. Nelson, and Shanhui Fan, *Phys. Rev. Lett.* **90**, 196402 (2003).
- [45] John David Jackson, *Classical Electrodynamics* (John Wiley & Sons, New York, 1975).
- [46] L. J. Wang, A. Kuzmich, and A. Dogariu, *Nature (London)* **406**, 277 (2000).
- [47] S. Longhi, P. Laporta, M. Belmonte, and E. Recami, *Phys. Rev. E* **65**, 046610 (2002).
- [48] Herbert G. Winful, *Phys. Rev. Lett.* **90**, 023901 (2003).
- [49] Amnon Yariv and Pochi Yeh, *Optical Waves in Crystals* (John Wiley & Sons, New York, 1984).
- [50] S. Datta, C. T. Chan, K. M. Ho, and C. M. Soukoulis, *Phys. Rev. B* **48**, 14 936 (1993).